PET/CT with ^{18}F-FDG– and ^{18}F-FBEM–Labeled Leukocytes for Metabolic Activity and Leukocyte Recruitment Monitoring in a Mouse Model of Pulmonary Fibrosis

Benjamin Bondue*[1,2], Félicie Sherer*[3,4], Gaetan Van Simaeys[3,4], Gilles Doumont[3,4], Dominique Egrise[3,4], Yousof Yakoub[5], François Huaux[5], Marc Parmentier[2], Sandrine Rorive[3], Sébastien Sauvage[3], Simon Lacroix[3,4], Olivier Vosters[2], Paul De Vuyst[1], and Serge Goldman[3,4]

[1]Service de Pneumologie, Hôpital Erasme, Université Libre de Bruxelles, Brussels, Belgium; [2]Institut de Recherche Interdisciplinaire en Biologie Humaine et Moléculaire (I.R.I.B.H.M.), Université Libre de Bruxelles, Brussels, Belgium; [3]Center for Microscopy and Molecular Imaging, Université Libre de Bruxelles, Gosselies, Belgium; [4]Service de Médecine Nucléaire, Hôpital Erasme, Université Libre de Bruxelles, Brussels, Belgium; and [5]Centre for Toxicology and Applied Pharmacology, Université Catholique de Louvain, Louvain-la-Neuve, Belgium

Idiopathic pulmonary fibrosis is characterized by a progressive and irreversible respiratory failure. Validated noninvasive methods able to assess disease activity are essential for prognostic purposes as well as for the evaluation of emerging antifibrotic treatments. **Methods:** C57BL/6 mice were used in a murine model of pulmonary fibrosis induced by an intratracheal instillation of bleomycin (control mice were instilled with a saline solution). At different times after instillation, PET/CT with ^{18}F-FDG– or ^{18}F-4-fluorobenzamido-*N*-ethylamino-maleimide (^{18}F-FBEM)–labeled leukocytes was performed to assess metabolic activity and leukocyte recruitment, respectively. **Results:** In bleomycin-treated mice, a higher metabolic activity was measured on ^{18}F-FDG PET/CT scans from day 7 to day 24 after instillation, with a peak of activity measured at day 14. Of note, lung mean standardized uptake values correlated with bleomycin doses, histologic score of fibrosis, lung hydroxyproline content, and weight loss. Moreover, during the inflammatory phase of the model (day 7), but not the fibrotic phase (day 23), bleomycin-treated mice presented with an enhanced leukocyte recruitment as assessed by ^{18}F-FBEM–labeled leukocyte PET/CT. Autoradiographic analysis of lung sections and CD45 immunostaining confirm the higher and early recruitment of leukocytes in bleomycin-treated mice, compared with control mice. **Conclusion:** ^{18}F-FDG– and ^{18}F-FBEM–labeled leukocyte PET/CT enable monitoring of metabolic activity and leukocyte recruitment in a mouse model of pulmonary fibrosis. Implications for preclinical evaluation of antifibrotic therapy are expected.

Key Words: pulmonary fibrosis; bleomycin; PET scan; fluorodeoxyglucose; disease monitoring

Idiopathic pulmonary fibrosis (IPF) is characterized by a progressive and irreversible replacement of functional lung parenchyma by a fibrous tissue. The prognosis for patients with IPF

is poor, with a 5-y survival rate worse than in several types of cancer and a median survival rate between 2 and 5 y (*1,2*). The etiology of IPF is unknown, but a role of environmental and genetic factors is suspected, resulting in repeated injuries of type II alveolar epithelial cells associated with an abundant and inappropriate fibrotic response (*1,3–5*). Inflammation is present in IPF lungs but does not seem to play a central role in the physiopathology of the disease as aggressive antiinflammatory therapies failed to improve IPF patients (*6*).

The diagnosis of IPF is difficult to establish, and a multidisciplinary approach is mandatory based on clinical, biologic, radiologic, and histologic data (*1*). To date, the severity of the disease is determined by the initial evaluation of symptoms, the level of functional and radiologic abnormalities, and the modifications of these parameters during a follow-up period in the range of months to years. Markers of the disease activity would be useful to determine the prognosis and the individual response of patients to therapeutic interventions.

A few recent studies evaluated the use of PET techniques in IPF patients (*7–15*), mostly with ^{18}F-FDG as a tracer of glucose uptake and metabolism. These studies showed that lungs from IPF patients present a clear enhancement of ^{18}F-FDG uptake, with an excellent short-term reproducibility (*11–14*). However, it is actually not known whether ^{18}F-FDG uptake is related to the severity of the fibrotic process and could be exploited for early assessment of antifibrotic therapies. By consequence, there is a strong need to further characterize PET imaging techniques in animal models of lung fibrosis. These models allow dose–response assessment for selected fibrotic triggers and direct comparison to histologic and biochemical ex vivo data. Animal experiments also permit repeated evaluation in the course of the pathophysiologic process and well-controlled testing of therapeutic interventions. Very few animal data evaluated the use of this technique in models of fibrotic lung diseases to date (*16–18*). The bleomycin-induced pulmonary fibrosis model is the most commonly used; it has the advantage of quickly inducing a strong fibrotic response after only a single intratracheal injection of bleomycin, beginning around day 14, with maximal responses generally noted around days 21–28 (*19,20*). This model also shares several common features with other types of fibrosis such as radiation-induced pulmonary fibrosis (*21*), thus enlarging its application field. However, the presence of a strong inflammatory reaction over the first week

(not observed in human IPF patients) is an important difference to be considered between the murine and the human IPF model. Applying this animal model for imaging development therefore requires testing of the respective contributions of inflammatory and fibrotic reactions to the images produced.

The aim of the present study was therefore to evaluate ^{18}F-FDG uptake at both the early inflammatory and the later fibrotic phases of the murine bleomycin-induced pulmonary fibrosis model. Because ^{18}F-FDG uptake can be related to either the fibrotic activity or the inflammatory process, we address the question about the contribution of leukocyte recruitment to the ^{18}F-FDG signal by a parallel analysis of pulmonary distribution of labeled leukocytes. For leukocyte labeling, we applied a recently developed method involving a radiolabeled probe, the ^{18}F-4-fluorobenzamido-*N*-ethylamino-maleimide (^{18}F-FBEM), covalently bound to thiol groups present on the cell surface of leukocytes (*22*). The relation between different doses of bleomycin, changes in lung collagen content, and level of ^{18}F-FDG uptake was also studied.

MATERIALS AND METHODS

Mice

Eight- to 10-wk-old C57BL/6 female mice (Charles River) were used throughout these studies. They were housed and bred in a specific-pathogen-free–like environment with access to food and water at will. A minimum of 8 mice in the bleomycin-treated group and 5 mice in the control group were used for each experiment ($n = 174$ animals). Some mice were used for both in vivo and ex vivo experiments. No mice were used for both the ^{18}F-FDG and the labeled leukocyte experiments. All procedures were reviewed and approved by the local committee for animal welfare.

Lung Fibrosis Model

To study the role of PET imaging in pulmonary fibrosis, the bleomycin model of pulmonary fibrosis was used as previously described (*23*). Briefly, mice were instilled with bleomycin (doses ranging from 0.005 to 0.02 U/60 μL/mouse; Sanofi Aventis) resuspended and diluted in sterile saline solution (0.9% NaCl). All instillations were performed on mice anesthetized with a mix of 1 mg of ketamine (Ketalar; Ceva) and 0.2 mg of xylazine (Rompun; Bayer AG). Control mice were treated with saline. At several times after instillation, mice were used for PET imaging or sacrificed for further investigations by exsanguination under deep isoflurane-induced anesthesia (4%isoflurane in 1 L/min O$_2$).

Quantitative Assessment of Lung Fibrosis

The Ashcroft score of lung fibrosis was used to assess the amount of fibrotic tissue (*24*). Briefly, unlavaged whole lungs were collected, inflated with 4% paraformaldehyde, and embedded in paraffin. Sections (7 μm thick) were prepared and stained with Masson trichrome for light microscopic examination. Fibrotic changes were scored for each lung by calculating the mean of the fibrotic changes on 5 different fields (magnification ×10).

Lung total collagen was estimated by measuring hydroxyproline (OH-proline), a specific component of collagen. Lungs were homogenized on ice with an Ultra-Turrax T25 homogenizer (Janke & Kunkel) and stored at −80°C. Whole-lung homogenate was hydrolyzed in HCl 6N at 108°C during 24 h, and OH-proline was quantified by high-performance liquid chromatography. Data were expressed as micrograms of OH-proline per lung. Cytokine (IL-6) and chemokine (CCL2) levels were also measured in the supernatant of lung homogenates using enzyme-linked immunosorbent assays (R&D Systems).

PET Imaging and Autoradiography

^{18}F-FDG PET/CT Imaging. The metabolic activity related to the bleomycin-induced pulmonary fibrosis was assessed with ^{18}F-FDG PET/CT imaging at 7, 14, 24, and 36 d after bleomycin instillation (0.02 U). In experiments evaluating the relationship between the ^{18}F-FDG uptake and the dose of bleomycin instilled, PET/CT imaging was performed at 7 and 14 d after instillation in 4 groups—3 groups were instilled with bleomycin (0.02, 0.01, and 0.005 U), and a control group was instilled with saline. Mice were fasted overnight. The ^{18}F-FDG was synthesized at the PET/Biomedical Cyclotron Unit of the Nuclear Medicine Department at ULB-Hôpital Erasme. Mice were injected intravenously (lateral tail vein) with about 3.9 MBq (SD, 0.39) of ^{18}F-FDG and kept under isoflurane anesthesia for 10 min after injection to limit tracer uptake within skeletal muscle and brown adipose tissue (*25*). PET/CT imaging was performed under isoflurane anesthesia 60 min after ^{18}F-FDG injection using a preclinical PET/CT tomograph (nanoPET-CT; Mediso). PET emission images were recorded for 15 min in 3-to-1 coincidence mode in normal counting rate. CT acquisition parameters were 55 kV for a tube current of 145 μA, 1,100 ms per projection, 180 projections per rotation, pitch of 1, a frame binning of 2 by 2, and a cubic reconstructed voxel size of 212 μm. Scaled CT images were used to obtain CT attenuation-corrected and scatter-corrected PET images. All PET images were also corrected for random counts, dead time, and decay. The PET acquisitions were reconstructed using a fully 3-dimensional iterative ordered-subset expectation maximization reconstruction algorithm (4 iterations, 6 subsets, intermediate regularization setting, median filtering period defined from iteration counts). Three-dimensional spheric regions of interest (12-pixel diameter) were drawn on pulmonary parenchyma in the left and right lung using InVivoScope2.0 (inviCRO). Care was taken not to include voxels close to the heart, which demonstrated a high ^{18}F-FDG uptake (Supplemental Fig. 1; available at http://jnm.snmjournals.org). Mean activity within each region of interest was expressed in Bq/mL and was subsequently divided by the ratio A_0 (injected activity decay-corrected at the start of the PET acquisition [Bq] to animal weight [g]) to provide
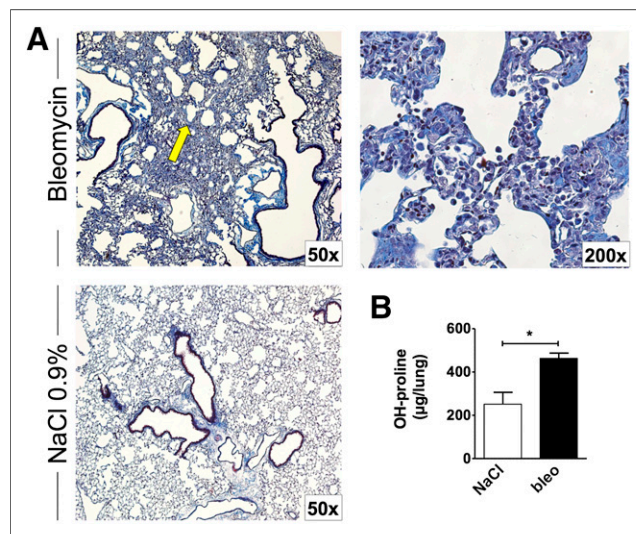
FIGURE 1. Bleomycin model of lung fibrosis. (A) Representative lung sections stained with Masson trichrome of C57BL/6 mice instilled with bleomycin (0.02U, upper) or saline solution (NaCl 0.9%, lower). Yellow arrow indicates honeycombing areas. (B) Lung OH-proline content at day 24 after instillation (mean ± SEM; control, $n = 3$; bleomycin, $n = 6$). Displayed data are representative of 3 independent experiments. *$P < 0.05$. Bleo = bleomycin.
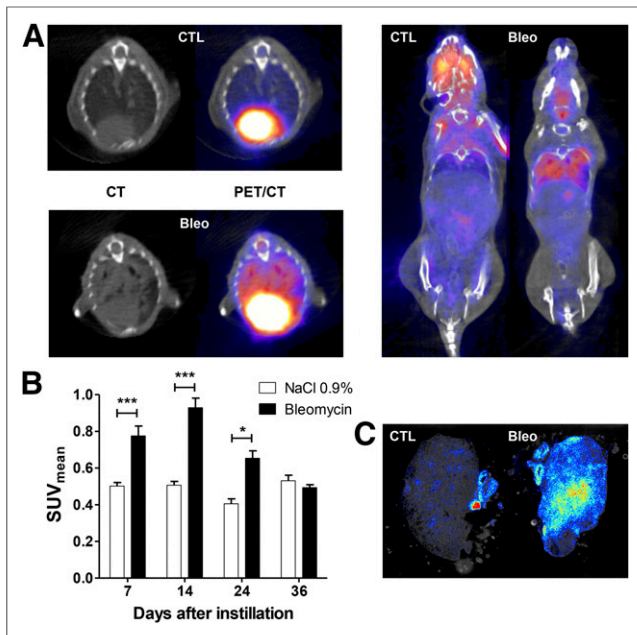
FIGURE 2. Increased ^{18}F-FDG uptake in bleomycin-treated mice. Bleomycin (0.02U)- and saline-treated mice were used for in vivo imaging by PET/CT scans 1 h after intravenous injection of 3.9 MBq in the tail. (A) Representative transverse (left) and coronal (right) sections obtained at day 14 after instillation. (B) Lung SUV$_{mean}$ measured 7, 14, 24, and 36 d after administration of NaCl 0.9% (CTL) or bleomycin (Bleo). Data shown are mean ± SEM and result from pooling of 3 independent experiments (bleomycin groups: n = 16, 17, 12, and 7; control group: n = 10, 12, 4, and 4 for days 7, 14, 24, and 36, respectively). (C) Representative autoradiography of OCT-embedded lung sections obtained at day 14 after instillation. *P < 0.05; ***P < 0.001.

a mean standardized uptake value (SUV$_{mean}$). For each mouse, the SUV$_{mean}$ for right and left lungs were averaged before statistical analysis was performed.

^{18}F-FBEM–Radiolabeled Leukocyte PET/CT Imaging. Leukocyte recruitment was assessed by means of PET/CT imaging of ^{18}F-FBEM–radiolabeled leukocytes at 7, 14, and 23 d and instillation. Preparation of ^{18}F-FBEM and its potential for cell labeling have been previously described (*22*). No lung retention of free ^{18}F-FBEM at 1 h after injection was observed in bleomycin-treated animals ((*22*); Supplemental Fig. 2). The leukocytes were obtained from the spleen of C57BL/6 mice, with expected proportions of lymphocytes, monocytes/macrophages, and neutrophils being 84%, 5%, and 2%, respectively (*26*). The cells were washed 2 times with Dulbecco phosphate-buffered saline (D-PBS) and centrifuged for 5 min at 200*g*. The cell pellet was suspended in D-PBS at a concentration of 25×10^6 cells per mL. ^{18}F-FBEM was synthesized at the PET/Biomedical Cyclotron Unit of ULB-Hôpital Erasme. ^{18}F-FBEM diluted in D-PBS was added to the cells, with a mean ^{18}F-FBEM activity of 40 MBq for 25×10^6 cells. After 30-min incubation at 37°C, the leukocytes were washed 3 times with D-PBS and centrifuged for 5 min at 200*g*, and the pellet was resuspended in D-PBS. PET/CT was performed 105 min after the intravenous injection (tail) of 4 million labeled leukocytes (0.5–2.63 MBq), these conditions having been established after dynamic acquisitions in preliminary experiments. PET emission images were recorded for 30 min in 3-to-1 coincidence mode in normal counting rate. CT acquisition and PET reconstruction parameters, as well as the region-of-interest–based quantification method, were identical to those applied for ^{18}F-FDG imaging.

Autoradiography. Immediately after PET/CT imaging, randomly selected mice were sacrificed by exsanguination under deep isoflurane-induced anesthesia. Lungs were collected and inflated with 800 μL of optimum-cutting-temperature (OCT) compound (Sakura Finetek). Lung samples were thereafter embedded in OCT compound and stored at −20°C. Frozen lung sections (8 μm) were cut in the sagittal plane with a cryostat (Shandon Cryotome FSE; Thermo). Numeric autoradiographic images of lung slices were acquired for 2 h with the Microimager M-40 (BiospaceLab).

Statistical Analysis

Significance was determined using the Student t test for single comparison or 1- and 2-way ANOVA with Bonferroni post hoc tests for multiple comparisons using the Prism5 software (GraphPad Software). For all tests, a P value of less than 0.05 was considered significant.

RESULTS

Significant Pulmonary Fibrosis After Single Administration of Bleomycin

At 24 d after instillation, bleomycin-treated mice showed important histologic modifications characterized by marked interstitial, peribronchiolar, and perivascular fibrosis; thickening of alveolar septa; leukocyte infiltrates; and important architectural disruption with honeycombing areas (Fig. 1A). At day 24 after instillation, lung OH-proline content was also determined from bleomycin- and saline-treated mice to assess their collagen content. Bleomycin-treated mice showed almost twice higher
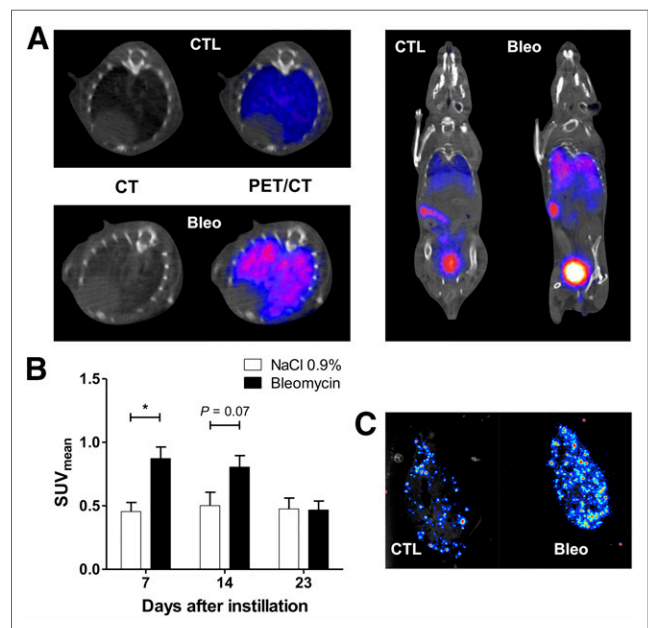
FIGURE 3. Increased presence of ^{18}F-FBEM–labeled leukocytes in bleomycin-treated lungs. Bleomycin (Bleo)- and saline (CTL)-treated mice were used for in vivo imaging of leukocyte recruitment by PET/CT scans 105 min after intravenous injection of 4 million ^{18}F-FBEM–labeled leukocytes in tail vein. (A) Representative transverse (left) and coronal (right) sections obtained at day 7 after instillation. (B) Lung SUV$_{mean}$ measured 7, 14, and 23 d after administration of NaCl 0.9% or bleomycin. Data shown are mean ± SEM and result from pooling of 2 independent experiments (bleomycin groups: n = 18, 17, and 14; control group: n = 6, 6, and 5 for days 7, 14, and 23, respectively). (C) Representative autoradiography of OCT-embedded lung sections obtained at day 7 after instillation. *P < 0.05.
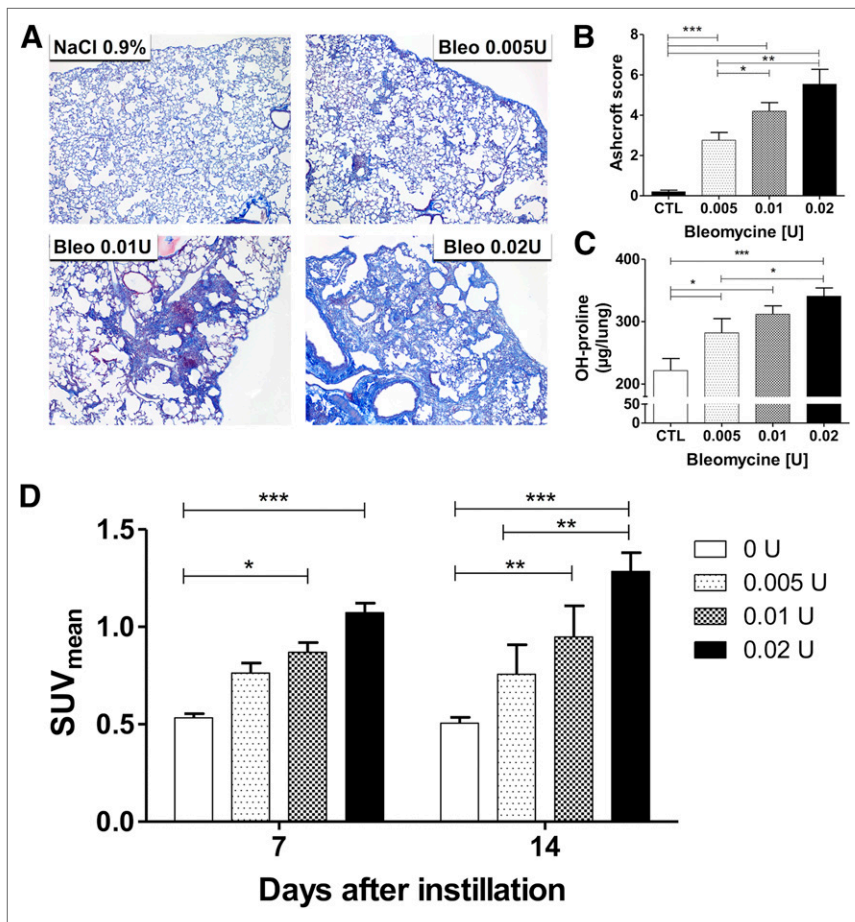
FIGURE 4. Positive correlation between bleomycin doses and ^{18}F-FDG uptake and pulmonary fibrosis. Experiments were conducted with doses of bleomycin ranging from 0.005 to 0.02 U. (A) Representative sections of lungs stained with Masson trichrome (magnification, ×20) obtained 21 d after instillation of NaCl 0.9%, bleomycin 0.005 U, bleomycin 0.01 U, and bleomycin 0.02 U. (B) Ashcroft score of fibrosis was measured at 21 d after instillation of bleomycin or NaCl 0.9% ($n = 5$ for each group, mean of 5 fields by animal). Lung OH-proline at day 16 after instillation (C) and lung SUV$_{mean}$ at days 7 and 14 after instillation (D) were assessed in bleomycin (0.02 U, $n = 12$; 0.01 U, $n = 8$; 0.005 U, $n = 7$) or control ($n = 4$) mice. Displayed data are mean ± SEM and are representative of 2 independent experiments. *$P < 0.05$; **$P < 0.01$; ***$P < 0.001$. Bleo = bleomycin; CTL = control.

OH-proline content than control mice (463 ± 24 vs. 251 ± 54 μg/lung, respectively, $P < 0.05$) (Fig. 1B). Altogether, these data confirmed the induction of a strong fibrotic response in the later phase of this model and allow its use in further PET experiments.

Increased ^{18}F-FDG Uptake in Bleomycin-Treated Mice

Compared with control mice, bleomycin (0.02 U)-treated mice showed a significantly higher ^{18}F-FDG uptake starting at day 7 after instillation (SUV$_{mean}$, 0.77 ± 0.05 vs. 0.50 ± 0.02; $P < 0.001$) and reaching a peak value at day 14 after instillation (SUV$_{mean}$, 0.93 ± 0.05 vs. 0.51 ± 0.02; $P < 0.001$) (Figs. 2A and 2B). Lung sections from the computed tomodensitometry showed strong alterations with important areas of lung consolidations in bleomycin-treated mice, compared with control mice (Fig. 2A). Moreover, the examination of the fusion images (PET and tomodensitometry) indicated that ^{18}F-FDG uptake was mostly noticed in consolidation areas of the lungs. The higher ^{18}F-FDG uptake in bleomycin-treated mice was still present at the late fibrotic phase of the disease, with a significant difference at day 24 (SUV$_{mean}$, 0.65 ± 0.04 vs.

0.41 ± 0.03; $P < 0.05$) whereas ^{18}F-FDG uptake became similar between groups at day 36 after instillation (SUV$_{mean}$, 0.49 ± 0.02 vs. 0.53 ± 0.03; $P =$ not significant). The ^{18}F-FDG uptake findings obtained with PET at the various time points were confirmed by autoradiographic analysis performed on lung sections obtained from control and bleomycin-treated mice showing higher count numbers in the bleomycin-treated mice than control mice (Fig. 2C; Supplemental Fig. 3).

Early Increase in Presence of ^{18}F-FBEM–Labeled Leukocytes in Lungs of Bleomycin-Treated Mice

In parallel to ^{18}F-FDG PET experiments, the recruitment of leukocytes was investigated during the inflammatory and the fibrotic phases of the model. Higher leukocyte recruitment was noticed at day 7 after bleomycin administration (SUV$_{mean}$, 0.87 ± 0.09 in the bleomycin group, compared with 0.45 ± 0.07 in the control group; $P < 0.05$) (Figs. 3A and 3B). At day 14, the difference became nonsignificant (SUV$_{mean}$, 0.80 ± 0.09 in the bleomycin group, compared with 0.50 ± 0.10 in the control group; $P = 0.07$) and, in contrast with the ^{18}F-FDG uptake data, it totally disappeared at day 23 (SUV$_{mean}$, 0.47 ± 0.07 in the bleomycin group, compared with 0.48 ± 0.09 in the control group; $P =$ not significant). The higher leukocyte recruitment observed with the PET method at 7 d after instillation was confirmed by autoradiographic analysis showing higher count numbers on lung sections from bleomycin-treated mice than control mice (Fig. 3C). These data are also in line with analysis of the cellularity of the bronchoalveolar lavage and lung CD45 immunostaining performed at several time points after bleomycin administration (Supplemental Fig. 4). These data highlight an early recruitment of inflammatory cells (first neutrophils then macrophages and lymphocytes) and a relative decrease in these inflammatory cells during the later fibrotic phase of the model at times when their recruitment, as assessed by ^{18}F-FBEM–labeled leukocytes, was similar in the 2 groups (Fig. 3B).

Correlation Between Bleomycin Doses, ^{18}F-FDG Uptake, Weight Loss, and Pulmonary Fibrosis

We investigated whether different doses of bleomycin could induce variable degrees of fibrosis and if there was a correlation between the degree of lung fibrosis and the mean lung standardized uptake values calculated from ^{18}F-FDG PET imaging. Doses of bleomycin ranging from 0.005 to 0.02 U were used and mice imaged at days 7 and 14 according to our previous results. These dose–response experiments showed a positive correlation between bleomycin dose and degree of fibrosis (assessed by histologic examination of lung sections and by the related Ashcroft score of fibrosis) (Figs. 4A and 4B), OH-proline content reflecting collagen
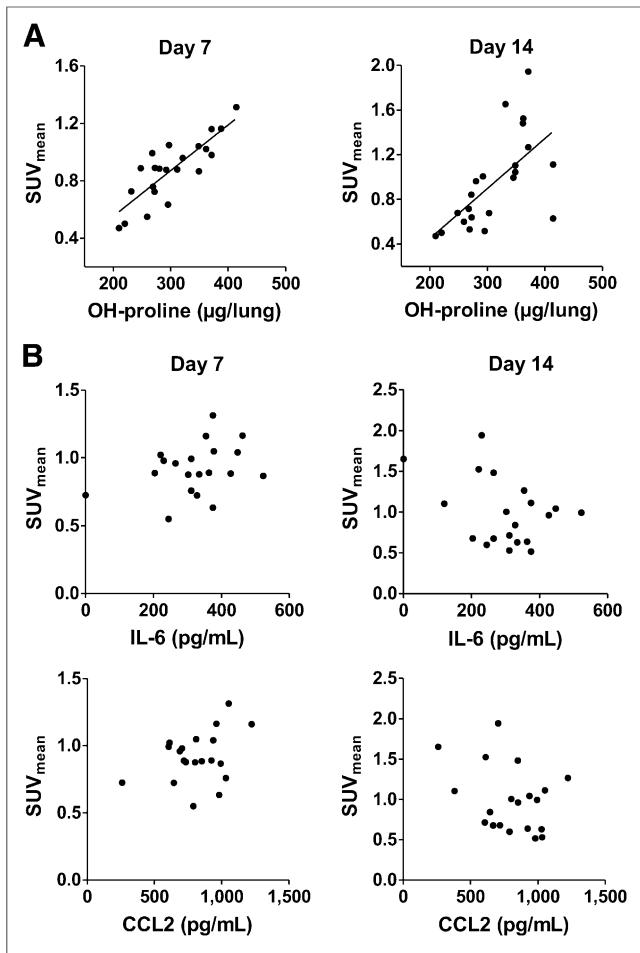
FIGURE 5. Correlation between ^{18}F-FDG uptake and pulmonary fibrosis but not with inflammatory markers. Correlation between marker of fibrosis (OH-proline) (A), markers of inflammation (IL-6 and CCL2) assessed in lung at day 16 after administration of different doses of bleomycin (B), and lung SUV$_{mean}$ measured at 7 d (left) and 14 d after bleomycin administration (right).

synthesis and deposition (Fig. 4C), and weight loss (Supplemental Fig. 5). Furthermore, at both time points (7 and 14 d after instillation), ^{18}F-FDG PET imaging showed a strong correlation between bleomycin dose and lung SUV$_{mean}$ (Fig. 4D). Analysis of the source of the variance indicated that the bleomycin dose accounted for 48% of the total variance, with a P value of less than 0.0001. Moreover, when the control group was eliminated, the bleomycin doses still accounted for 28% of the total variance, with a P value of 0.0034. An important correlation was also found between lung SUV$_{mean}$ and OH-proline content ($r^2 = 0.68$ and 0.40 at days 7 and 14, respectively; $P < 0.01$) (Fig. 5A). Conversely, no correlation was observed between the inflammatory chemokine CCL2, the cytokine IL-6, and the ^{18}F-FDG uptake at days 7 and 14 after the bleomycin treatment (Fig. 5B).

DISCUSSION

IPF is a severe disease with an often-fatal outcome. IPF results from abnormal or uncontrolled lung repair processes and is characterized by a disorganized and remodeled lung interstitium accompanied by an excessive production of extracellular matrix proteins. The end result of this process is an irreversible loss of lung compliance and impaired gas exchange. Validated noninvasive methods able to assess disease activity are essential for prognostic purpose as well as for the evaluation of emerging antifibrotic treatments. Presently, no functional imaging technique or biomarker allows noninvasive, precise, and immediate evaluation of disease activity and severity. Therefore, the aim of this study was to investigate the utility of ^{18}F-FDG to assess metabolic activity in an animal model of lung fibrosis. In the well-characterized bleomycin model we used, after a neutrophilic and lymphocytic alveolitis occurring within the first week of the toxic insult to the alveolar epithelium, inflammatory cells were cleared, fibroblasts proliferated, and extracellular matrix was synthesized in excess (19,20). Fibrosis was detected biochemically and histologically by day 14, with maximal responses noted around days 21–28.

Our results demonstrate that ^{18}F-FDG uptake increases early during the inflammatory phase of the disease and persists in the later fibrotic phase. These results are in line with data from the only previous animal ^{18}F-FDG PET study on lung fibrosis, performed in a rabbit model of this condition (16). In their study, Jones et al. showed a peak of ^{18}F-FDG uptake 28 h after instillation of bleomycin correlating at the inflammatory phase of the disease with recruitment of lung neutrophils. Then, the ^{18}F-FDG uptake slowly decreased but remained significantly high up to 30 d after the bleomycin treatment (16).

To evaluate to what extent the inflammatory burst participated in the enhanced ^{18}F-FDG uptake, we have compared the kinetics of ^{18}F-FDG– and ^{18}F-FBEM–radiolabeled leukocyte pulmonary uptake. Our data demonstrate an early increase in leukocyte recruitment and a return to normal values in the fibrotic phase of the disease, contrasting with the prolonged increase in ^{18}F-FDG uptake. These imaging data are in line with the model description (19) and confirmed by our bronchoalveolar lavage cytologic and lung immunohistologic data. We then concluded that the early increase in ^{18}F-FDG uptake was likely related to the early recruitment of leukocytes and associated inflammation.

Conversely, on the basis of the ^{18}F-FBEM–radiolabeled leukocyte findings, the persistence of a high ^{18}F-FDG uptake in the fibrotic phase of the model is not explained by an active recruitment of leukocytes. We hypothesized, therefore, that it rather reflected the fibrotic process itself, even if a minor contribution of a residual inflammatory activity remained plausible. This interpretation is supported by experiments with varying doses of bleomycin. These show a strong positive correlation between ^{18}F-FDG lung uptake and OH-proline content, a biochemical marker of synthesis and deposition of collagen. Such a correlation is not observed between ^{18}F-FDG uptake and inflammatory cytokines and chemokines. Consistent with our findings, human ^{18}F-FDG PET/CT data have demonstrated that the sites of maximal ^{18}F-FDG uptake in IPF correspond to CT changes, with predominant reticulation and honeycombing, which are classically associated with fibrotic changes, rather than with ground-glass opacities, more classically associated with inflammatory changes (11). From a cellular point of view, the late ^{18}F-FDG uptake probably results from a high glucose consumption in proliferating fibroblasts or collagen-producing myofibroblasts. Interestingly, such an effect has been evidenced in tumor-associated fibroblasts, with an increase in hydrogen peroxide concentration in the tumor microenvironment driving the enhanced

glucose uptake by fibroblasts under oxidative stress (27). Recent studies have emphasized the role of the oxidative stress as a key player in the establishment and progression of pulmonary fibrosis in animal models and possibly in human IPF (28,29). Therefore, ^{18}F-FDG uptake in these conditions might actually reflect the pathophysiologic process engaged. In 1 previous report, it has been suggested that ^{18}F-FDG uptake in human IPF could result from a relative increase in pulmonary blood volume, because erythrocytes express glucose transporter type 1 (10). This hypothesis seems unlikely in our model because ^{18}F-FDG uptake is clearly demonstrated on autoradiographic images of exsanguinated lungs.

CONCLUSION

Our data strongly suggest that ^{18}F-FDG uptake is related to the fibrotic process of interest in an animal model of lung fibrosis. Still, in the early phase of the model, inflammation probably affects the PET/CT results.

These findings position ^{18}F-FDG PET imaging as a potential method for the noninvasive evaluation of disease activity in IPF and other forms of fibrosis. ^{18}F-FDG PET emerges as a promising tool to select patients for therapeutic interventions and to assess response to therapy. Further animal studies and clinical trials are necessary to validate this application of ^{18}F-FDG PET/CT.

DISCLOSURE

ACKNOWLEDGMENTS

REFERENCES

1. Raghu G, Collard HR, Egan JJ, et al. An official ATS/ERS/JRS/ALAT statement: idiopathic pulmonary fibrosis: evidence-based guidelines for diagnosis and management. *Am J Respir Crit Care Med.* 2011;183:788–824.

2. Bjoraker JA, Ryu JH, Edwin MK, et al. Prognostic significance of histopathologic subsets in idiopathic pulmonary fibrosis. *Am J Respir Crit Care Med.* 1998;157:199–203.

3. Günther A, Korfei M, Mahavadi P, von der Beck D, Ruppert C, Markart P. Unravelling the progressive pathophysiology of idiopathic pulmonary fibrosis. *Eur Respir Rev.* 2012;21:152–160.

4. Kropski JA, Lawson WE, Young LR, Blackwell TS. Genetic studies provide clues on the pathogenesis of idiopathic pulmonary fibrosis. *Dis Model Mech.* 2013;6:9–17.

5. Selman M, Pardo A. Role of epithelial cells in idiopathic pulmonary fibrosis: from innocent targets to serial killers. *Proc Am Thorac Soc.* 2006;3:364–372.

6. Idiopathic Pulmonary Fibrosis Clinical Research Network. Raghu G, Anstrom KJ, King TE, Lasky JA, Martinez FJ. Prednisone, azathioprine, and N-acetylcysteine for pulmonary fibrosis. *N Engl J Med.* 2012;366:1968–1977.

7. Ambrosini V, Zompatori M, De Luca F, et al. ^{68}Ga-DOTANOC PET/CT allows somatostatin receptor imaging in idiopathic pulmonary fibrosis: preliminary results. *J Nucl Med.* 2010;51:1950–1955.

8. Lavalaye J, Grutters JC, van de Garde EMW, et al. Imaging of fibrogenesis in patients with idiopathic pulmonary fibrosis with cis-4-[^{18}F]-fluoro-L-proline PET. *Mol Imaging Biol.* 2009;11:123–127.

9. Bellani G, Cairoli P. Lung imaging during acute respiratory distress syndrome: CT- and PET-scanning. *Trends Anaesth Crit Care.* 2011;1:203–209.

10. El-Chemaly S, Malide D, Yao J, et al. Glucose transporter-1 distribution in fibrotic lung disease: association with [^{18}F]-2-fluoro-2-deoxyglucose-PET scan uptake, inflammation, and neovascularization. *Chest.* 2013;143:1685–1691.

11. Groves AM, Win T, Screaton NJ, et al. Idiopathic pulmonary fibrosis and diffuse parenchymal lung disease: implications from initial experience with ^{18}F-FDG PET/CT. *J Nucl Med.* 2009;50:538–545.

12. Meissner H-H, Soo Hoo GW, Khonsary SA, Mandelkern M, Brown CV, Santiago SM. Idiopathic pulmonary fibrosis: evaluation with positron emission tomography. *Respiration.* 2006;73:197–202.

13. Umeda Y, Demura Y, Ishizaki T, et al. Dual-time-point ^{18}F-FDG PET imaging for diagnosis of disease type and disease activity in patients with idiopathic interstitial pneumonia. *Eur J Nucl Med Mol Imaging.* 2009;36:1121–1130.

14. Win T, Lambrou T, Hutton BF, et al. ^{18}F-fluorodeoxyglucose positron emission tomography pulmonary imaging in idiopathic pulmonary fibrosis is reproducible: implications for future clinical trials. *Eur J Nucl Med Mol Imaging.* 2012;39:521–528.

15. Win T, Screaton NJ, Porter J, et al. Novel positron emission tomography/computed tomography of diffuse parenchymal lung disease combining a labeled somatostatin receptor analogue and 2-deoxy-2[^{18}F]fluoro-D-glucose. *Mol Imaging.* 2012;11:91–98.

16. Jones HA, Schofield JB, Krausz T, Boobis AR, Haslett C. Pulmonary fibrosis correlates with duration of tissue neutrophil activation. *Am J Respir Crit Care Med.* 1998;158:620–628.

17. Jones HA, Valind SO, Clark IC, et al. Kinetics of lung macrophages monitored in vivo following particulate challenge in rabbits. *Toxicol Appl Pharmacol.* 2002;183:46–54.

18. Wallace WE, Gupta NC, Hubbs AF, et al. Cis-4-[^{18}F]fluoro-L-proline PET imaging of pulmonary fibrosis in a rabbit model. *J Nucl Med.* 2002;43:413–420.

19. Janick-Buckner D, Ranges GE, Hacker MP. Alteration of bronchoalveolar lavage cell populations following bleomycin treatment in mice. *Toxicol Appl Pharmacol.* 1989;100:465–473.

20. Moore BB, Hogaboam CM. Murine models of pulmonary fibrosis. *Am J Physiol Lung Cell Mol Physiol.* 2008;294:L152–L160.

21. Haston CK, Travis EL. Murine susceptibility to radiation-induced pulmonary fibrosis is influenced by a genetic factor implicated in susceptibility to bleomycin-induced pulmonary fibrosis. *Cancer Res.* 1997;57:5286–5291.

22. Lacroix S, Egrise D, Van Simaeys G, et al. [^{18}F]-FBEM, a tracer targeting cell-surface protein thiols for cell trafficking imaging. *Contrast Media Mol Imaging.* 2013;8:409–416.

23. Arras M, Louahed J, Heilier J-F, et al. IL-9 protects against bleomycin-induced lung injury: involvement of prostaglandins. *Am J Pathol.* 2005;166:107–115.

24. Ashcroft T, Simpson JM, Timbrell V. Simple method of estimating severity of pulmonary fibrosis on a numerical scale. *J Clin Pathol.* 1988;41:467–470.

25. Fueger BJ, Czernin J, Hildebrandt I, et al. Impact of animal handling on the results of ^{18}F-FDG PET studies in mice. *J Nucl Med.* 2006;47:999–1006.

26. Yang M, Büsche G, Ganser A, Li Z. Morphology and quantitative composition of hematopoietic cells in murine bone marrow and spleen of healthy subjects. *Ann Hematol.* 2013;92:587–594.

27. Martinez-Outschoorn UE, Lin Z, Trimmer C, et al. Cancer cells metabolically "fertilize" the tumor microenvironment with hydrogen peroxide, driving the Warburg effect: implications for PET imaging of human tumors. *Cell Cycle.* 2011;10:2504–2520.

28. Manoury B, Nenan S, Leclerc O, et al. The absence of reactive oxygen species production protects mice against bleomycin-induced pulmonary fibrosis. *Respir Res.* 2005;6:11–22.

29. Bocchino M, Agnese S, Fagone E, et al. Reactive oxygen species are required for maintenance and differentiation of primary lung fibroblasts in idiopathic pulmonary fibrosis. *PLoS ONE.* 2010;5:e14003.